Neurotherapeutics (2021) 18:1798–1814
https://doi.org/10.1007/s13311-021-01068-9

ORIGINAL ARTICLE

Specific Blockade of Bone Morphogenetic Protein-2/4 Induces Oligodendrogenesis and Remyelination in Demyelinating Disorders

Karin Mausner-Fainberg[1] · Moshe Benhamou[1,2] · Maya Golan[1] · Nadav Bleich Kimelman[4] · Uri Danon[4] · Ehud Marom[4] · Arnon Karni[1,2,3]

Accepted: 31 May 2021 / Published online: 22 June 2021

Abstract

Oligodendrocyte precursor cells (OPCs) are present in demyelinated lesions of multiple sclerosis (MS) patients. However, their differentiation into functional oligodendrocytes is insufficient, and most lesions evolve into nonfunctional astroglial scars. Blockade of bone morphogenetic protein (BMP) signaling induces differentiation of OPCs into myelin-producing oligodendrocytes. We studied the effect of specific blockade of BMP-2/4 signaling, by intravenous (IV) treatment with anti-BMP-2/4 neutralizing mAb in both the inflammatory model of relapsing experimental autoimmune encephalomyelitis (R-EAE) and the cuprizone-toxic model of demyelination in mice. Administration of anti-BMP-2/4 to R-EAE-induced mice, on day 9 post-immunization (p.i.), ameliorated R-EAE signs, diminished the expression of phospho-SMAD1/5/8, primarily within the astrocytic lineage, increased the numbers of de novo immature and mature oligodendrocytes, and reduced the numbers of newly generated astrocytes within the spinal cord as early as day 18 p.i. This effect was accompanied with elevated remyelination, manifested by increased density of remyelinating axons ($0.8 < \text{g-ratios} < 1$), and reduced fully demyelinated and demyelinating axons, in the anti-BMP-2/4-treated R-EAE mice, studied by electron microscopy. No significant immunosuppressive effect was observed in the CNS and in the periphery, during the peak of the first attack, or at the end of the experiment. Moreover, IV treatment with anti-BMP-2/4 mAb in the cuprizone-challenged mice augmented the numbers of mature oligodendrocytes and remyelination in the corpus callosum during the recovery phase of the disease. Based on our findings, the specific blockade of BMP-2/4 has a therapeutic potential in demyelinating disorders such as MS, by inducing early oligodendrogenesis-mediated remyelination in the affected tissue.

Keywords Bone morphogenetic proteins · Oligodendrogenesis · Remyelination · Demyelination · Experimental autoimmune encephalomyelitis · Cuprizone

Introduction

The pathological hallmarks of multiple sclerosis (MS) are lesions with inflammatory cell infiltration and focal demyelination, while axonal injury and oligodendroglial loss can occur as a primary phenomenon or secondary to the demyelination [1–6]. Oligodendrocyte regeneration and myelin repair are an important goal of therapy [7] because they restore the salutatory conduction of the action potential and prevent axonal and neuronal degeneration [8–10]. In most patients, lesion repair is limited, although the lesions may be populated by oligodendrocyte precursor cells (OPCs) [11–16]. OPCs derived from the subventricular zone (SVZ) of the lateral ventricles (LVs) [17–20] and from parenchymal OPCs [21] have been reported to regenerate into

Karin Mausner-Fainberg, Moshe Benhamou contributed equally to this work

✉ Arnon Karni
arnonk@tlvmc.gov.il

1 Neuroimmunology Laboratory, Neuroimmunology and Multiple Sclerosis Unit, Neurology Division, Tel Aviv Sourasky Medical Center, 6 Weizmann Street, 6423906 Tel Aviv, Israel

2 Sackler's Faculty of Medicine, Tel Aviv University, Tel Aviv, Israel

3 Sagol School of Neuroscience, Tel Aviv University, Tel Aviv, Israel

4 Stem Cell Medicine Ltd, Jerusalem, Israel

myelinating oligodendrocytes and repair demyelination, mainly in rodents. Indeed, remyelination may occur in MS lesions [22–24], even extensively in some cases [25, 26], but these OPCs often fail to differentiate into functionally active remyelinating oligodendrocytes in demyelinating lesions in rodents [27–29] and in human MS lesions [12, 30]. Instead, the affected lesions are populated by large numbers of reactive astrocytes that form a nonfunctional glial scar [4, 31, 32].

Bone morphogenetic proteins (BMPs) are growth factors that belong to the transforming growth factor beta (TGF-β) superfamily and are known to promote the differentiation of neural stem cells (NSCs) into astrocytes at the expense of their differentiation into oligodendrocytes or neurons in the adult central nervous system (CNS) [33–40]. Therefore, the blockade of BMP signaling is a possible target to induce oligodendrogenesis and remyelination. Indeed, CNS infusion of the BMP antagonists, noggin and chordin, increases the number of SVZ-derived OPCs and their mobilization into the corpus callosum (CC) in animal models of demyelination induced by cuprizone [41] and lysolecithin [42], respectively. Increased BMP expression was observed in animals with demyelination pathology induced by either cuprizone [41], ethidium bromide [43], or lysolecithin [44]. Moreover, elevated levels of BMPs were detected in the lumbar spinal cords of animals with myelin oligodendrocyte glycoprotein (MOG)-induced experimental autoimmune encephalomyelitis (EAE) [45] and in demyelinating lesions in postmortem brain tissues of patients with MS [46, 47]. In our previous studies, peripheral blood mononuclear cells, and particularly T cells, from patients with relapsing–remitting MS (RR-MS) secreted elevated levels of BMP-2, BMP-4, and BMP-5 [48], accompanied by reduced levels of the BMP antagonists noggin and follistatin [49, 50]. We have also found that the sera of patients with RR-MS contain elevated levels of BMP-2 [51]. Based on these data, the excessive and dysregulated presence of BMPs in the CNS of patients with MS may contribute to the failure of OPCs to mature into myelinating oligodendrocytes. Most of the abovementioned reports highlight either BMP-4 as the key player associated with demyelinated pathology [41, 43, 44] or both BMP-2 and BMP-4 [52]. Furthermore, noggin, which is a pro-remylinating BMP antagonist [41], has a higher affinity to BMP-2 and BMP-4, compared to BMP-5, BMP-6, and BMP-7 [53, 54]. Therefore, we hypothesized that specific blockade of BMP-2/4 signaling may be a potential therapeutic target for the induction of oligodendrocyte regeneration and remyelination.

In this study, we examined the therapeutic potential of an IV treatment with anti-BMP-2/4 neutralizing monoclonal antibody (mAb) in both R-EAE, the murine model of the inflammatory demyelinating disease, and in the non-inflammatory cuprizone-induced toxic model of demyelination. We studied the ability of this treatment to induce oligodendrogenesis and remylination in both of these models, as well as its ability to suppress immune activity in mice with R-EAE.

Materials and Methods

Induction of R-EAE and Treatment with Anti-BMP-2/4 mAb

Female SJL/JCrHsd mice (6–7 weeks of age) were purchased from Envigo Inc., Israel. Animal experimentation was approved by the Institutional Animal Care and Use Committee of Tel Aviv Sourasky Medical Center. The studies were conducted in accordance with the United States Public Health Service's Policy on Humane Care and Use of Laboratory Animals.

R-EAE was induced by subcutaneous immunization (day 0) with 100 μg of $PLP_{139-151}$ (Sigma-Aldrich Israel Ltd., Rehovot, Israel) in 0.1 ml of PBS per mouse. The peptide was emulsified in an equal volume of complete Freund's Adjuvant (CFA, Sigma-Aldrich, St Louis, MD) containing 500 μg of *Mycobacterium tuberculosis* H37RA (BD, Sparks, MD). The mice also received an intraperitoneal (IP) injection of 300 ng of pertussis toxin (PTX, from Sigma-Aldrich) in 0.2 ml of PBS. A second injection of PTX (300 ng/mouse) was administered 48 h later. The mice were randomly divided into 3 groups. Initial number of mice/group until day 14 post-immunization (p.i.) was 23. Then, 3 mice/group were scarified for the inflammation assessment, so between days 14 and 18 p.i., there were 20 mice/group. On day 18 p.i., 3 mice/group were sacrificed for immunohistochemical analysis and another 5 mice/group were sacrificed for electron microscopy analysis, so from that day until the end of the experiment, on day 41, there were 12 mice/group. The identities of the scarified mice were determined a priori, on the day the study groups were randomly divided (day 0).

Preliminary experiments were done to determine the dose of the treatment. The treatment was given on day 9 p.i.; the first day that the disease signs were seen. One group of R-EAE-induced mice was IV injected with 15 μg or 30 μg of the neutralizing Ab; mouse anti-human BMP-2/BMP-4 mAb (MAB3552, R&D Systems, Minneapolis, MN). This antibody has been demonstrated, by the manufacture to neutralize both human BMP-2- and human BMP-4-induced activity in the ATDC5 mouse chondrogenic cell line. The antibody neutralizes both human and mouse, BMP-2 and BMP-4 proteins, due to the relatively high homology between BMP-2 and BMP-4 in the ligand domain, as well as between the human and the mouse BMPs [55]. A control group of R-EAE-induced mice was IV injected with 15 μg or 30 μg of mouse IgG1 (MAB002) and served as isotype control (IC)-treated group. Another group of R-EAE-induced

mice was IV injected with PBS alone and served as the vehicle control group. Three mice in each group were daily IP injected with 1 mg/mouse of bromo-2′-deoxyuridine (BrdU, Sigma-Aldrich), starting on day 9, for the following 9 days, and were sacrificed on day 18 p.i. for immunohistochemical staining of the lumbar spinal cord sections. All mice were daily monitored for signs of EAE, and the observations were scored as follows: 0 = no disease, 1 = tail paralysis, 2 = hind limb weakness, 3 = hind limb paralysis, 4 = hind limb plus forelimb paralysis, and 5 = moribund.

Induction of the Cuprizone Model and Treatment with the Anti-BMP-2/4 Ab

Eight-week-old C57BL/6 male mice (Envigo Inc.) were fed with 0.2% cuprizone (w/w: bis-cyclohexanone-oxaldihydrazone, TD.140804, Teklad diet, Envigo Inc.) for 5 weeks (day 35, maximum demyelination) and then transferred to a regular diet. The mouse anti-human BMP-2/4 neutralizing mAb (MAB3552, R&D Systems) was administered via IV injection (30 µg/mouse) on day 15 after the initiation of the cuprizone diet. Control groups were IV injected with 30 µg/mouse of the corresponding IC (mouse IgG1, MAB002, R&D Systems) or vehicle alone (PBS). Mice were sacrificed 10 days after resuming the regular diet (recovery phase, day 46). Five animals per group were examined.

Immunohistochemistry

Mice were sacrificed, transcardially perfused with PBS and then with 4% paraformaldehyde (PFA). Brains and spinal cords were removed and fixed with 4% PFA overnight. Tissues were then cryoprotected with 30% sucrose in PBS overnight at 4 °C. Fixed tissues were embedded in OCT-Tissue Freezing Medium (Scigen Scientific, Gardena, CA) and frozen on dry ice. For R-EAE-induced mice experiments, sections were performed in the lumbar spinal cord (anterior/lateral funiculus), whereas for cuprizone model experiments the brain tissues were sectioned in the medial corpus callosum (−0.94 to −1.70 mm bregma). Cross Sects. (10 µm) were placed on X-tra adhesive slides (Leica Biosystems, Peterborough, UK) and stored at −20 °C. Sections were pre-incubated with a blocking solution containing 0.5% Tween 20 (Sigma-Aldrich), 1% bovine serum albumin (BSA, Sigma-Aldrich), and 3% horse serum (Gibco by Life Technologies, New York, NY) for 1 h and then incubated overnight at 4 °C with primary antibodies. The primary rat anti-BrdU Ab (1:200, [BU1/75(ICR1)], Abcam, Cambridge, MA) and the Alexa Fluor 594-conjugated donkey anti-rat IgG secondary Ab (1:200, Molecular Probes by Life Technologies, Waltham, MA, USA) were used to detect BrdU-labeled cells. The following primary antibodies were used to detect specific cell types: goat anti mouse PDGFR-α (AF1062, 1:10,R&D Systems), mouse anti-mature oligodendrocyte marker APC (Ab-7), clone CC-1 (OP80, 1:50, EMD Millipore Corporation, Temecula, CA), chicken anti-GFAP (NBP1-05,198, 1:250, Novus Biologicals, Littleton, Colorado), anti-MBP (ab40390, 1:750, Abcam), rabbit anti-oligodendrocyte transcription factor 2 (Olig-2) Ab (AB9610, 1:200, EMD Millipore) or goat anti-Olig-2 Ab (AF2418, 1:15, R&D Systems), phospho-Smad1/Smad5/Smad9 (Smad 8) rabbit mAb (D5B10,1:100, Cell Signaling Technology, MA, USA), rabbit anti-Neurofilament M (AB1987, 1:200, Merck) and goat anti-mouse CD45 Ab (AF114, 1:14, R&D Systems). The sections were incubated with Alexa Fluor® 488-conjugated anti-mouse or anti-rabbit or ant-goat IgG, or with Alexa Fluor® 633-conjugated anti-rabbit or anti-chicken IgG, or anti-chicken IgG, or with Alexa Fluor® 594-conjugated anti-rat or anti-goat or anti-rabbit IgG secondary antibodies, for 1 h (1:200; Molecular Probes by Life Technologies). For myelin detection, slides were also stained with Fluoromyelin green fluorescent (F34651, 1:300, Molecular Probes). Control slides were incubated with the secondary antibody alone. Stained sections were examined and photographed using an LSM 700 confocal microscope (Zeiss). Digital images were collected, and the number of double-positive cells was determined in 6–8 sections from each mouse; 3 mice were analyzed from each group. The number of double-positive cells was quantified using *ImageJ* software and calculated as the number of cells/mm^2. Single-stained cells were also quantified using *ImageJ* software and are presented as the percentage of the stained area.

Electron Microscopy

R-EAE-induced mice were sacrificed on day 18 p.i. and transcardially perfused with PBS and then with 2.5% glutaraldehyde (GA) + 2.5% PFA. Spinal cords were removed, and lumbar segments were fixed with 2.5% GA in PBS overnight at 4 °C. After several washes in PBS tissues were post-fixed in 1% osmium tetroxide (OsO_4) in PBS for 2 h at 4 °C. Dehydration was carried out in graded ethanol followed by embedding in glycid ether 100 (Serva, Heidelberg, Germany). In order to determine accurate location of EAE lesions for EM analysis, sections from lower lumbar spinal cord were first stained with hematoxylin and observed under light microscopy for inflammatory infiltrate area. Thin transverse sections from the same location of the lumbar spinal cord were mounted on formvar/carbon-coated grids, stained with uranyl acetate and lead citrate and examined in Jeol 1400 – Plus transmission electron microscope (Jeol, Japan). Images were captured using SIS Megaview III and iTEM the Tem imaging platform (Olympus).

Electron micrograph quantification of myelinated and vesiculated axons was performed on six images (×6000) per animal, 5 mice/group. The g-ratios, i.e., the ratio between

the axon diameter and the axon plus the myelin sheath diameter, were calculated using *Image J software*. Due to the variety orientation of the axons, which often do not exhibit a round shape in the sections, the inner and outer diameters were obtained from the axon area calculation. Moreover, axons that demonstrated vesicles within the inner myelin sheath, which represent early myelin structure breakdown, were analyzed, as previously described [56]. Analysis was performed on at least 200 fibers/animal.

Isolation of Mononuclear Cells from the Brain and Spinal Cord and Flow Cytometry

Mononuclears cells (MNCs) were isolated from the brains and spinal cords of 3 mice from each group on days 14 and 41 p.i. using a 70%/30% (vol/vol) Percoll gradient as previously described [57]. Viable cells were counted via the 0.4% trypan blue exclusion method using an automatic cell counter (NanoEntek).

Brain- and spinal cord-derived MNCs or splenocytes were incubated with anti-mouse CD45 APC-eFluor® 780, anti-mouse CD4 FITC, anti-mouse CD8a PE, anti-mouse CD11b APC, and anti-mouse CD19 PerCP-Cy5 (all from eBioscience by Thermo Fisher Scientific, San Diego, CA). Splenocytes (2×10^6 cells/ml) were cultured with the Cell Stimulation Cocktail (plus protein transport inhibitors, 500×, eBioscience) for 16 h to detect Th1, Th2, and Th17 cells. Cultures were then harvested and stained with anti-mouse CD45 APC-eFluor® 780, anti-mouse CD3 eFluor® 450, and anti-mouse CD4 FITC. Next, cells were fixed, permeabilized, and stained with anti-mouse IFN-γ APC for Th1 cells, anti-mouse IL-4 PE-Cy7 for Th2 cells, and anti-mouse/Rat IL-17A PE for Th17 cells (eBioscience). Treg cells among splenocytes were detected using the Mouse Regulatory T Cell Staining kit (eBioscience) according to the manufacturer's instructions. Flow cytometry analyses were performed on the FACSCanto II instrument (BD Bioscience), and the results were analyzed using *FlowJo software*. Cells in the $CD45^+$ gate were analyzed. Absolute numbers of $CD4^+$ T cells, $CD8^+$ T cells, monocytes, B cells and Tregs were calculated based on the numbers of total living cells.

Isolation of Splenocytes and Proliferation Assay An XTT proliferation assay was performed on splenocytes isolated from R-EAE groups on day 41 ($N=4$ mice per group), using an XTT kit (Biological Industries, Beit-Haemek, Israel). Briefly, splenocytes were isolated by straining mashed spleen through a 70-μm cell strainer into RPMI-1640 medium containing 10% FBS. Cells were cultured in 96-well plates (100,000/well) and either unstimulated or stimulated with 10 μg/ml purified plate-bound anti-mouse CD3e (145-2C11), the corresponding IgG IC (both from eBioscience), or 10 μg/ml suspended $PLP_{139-151}$ (Sigma-Aldrich Israel, Ltd.) for 72 h. Then, the XTT reaction solution was added, and the absorbance of the colored product was quantified after 4 h at a wavelength of 450 nm using a Thermo Max ELISA reader.

Statistical Analysis

Data are presented as the means ± standard errors of the means (SEM). The EAE severity was compared between groups using the Mann–Whitney *U* test. The null hypothesis asserted that the medians of the groups of samples were identical. The *U* values were calculated for the groups and for the conditions refuting the null hypothesis when $P<0.05$. For EM analysis, axons were grouped according to: g-ratio < 0.8, 0.8 < g-ratio < 1, and g-ratio = 1. These results were analyzed by chi-square test with Yates correction. A two-tailed Student's *t* test was conducted for all other experiments. Statistical significance was set to $P<0.05$.

Results

IV Treatment with an Antibody Directed Against BMP-2 and BMP-4 Ameliorates the Disease Severity of R-EAE

Our first objective was to examine the effect of systemic blockade of BMP-2/4 signaling in the R-EAE model, induced in SJL mice by PLP peptide immunization. We first examined the neutralization capacity of this anti-BMP-2/4 mAb in P19-neural cell differentiation model in vitro that was previously described [58]. Indeed, addition of anti-BMP-2/4 Ab, to P19 culture, in the presence of retinoic acid (RA) and rhBMP-2, reversed the neuronal phenotype acquisition of MAP-2 and blocked the astrogenesis, as examined by the marker GFAP (supplementary data, Fig. 1).

In a preliminary experiment we compared the doses of anti-BMP-2/4 neutralizing mAb (15 μg/mouse or 30 μg/mouse) and found a superior clinical effect of 30 μg/mouse (data not shown). Anti-BMP-2/4 neutralizing mAb (30 μg/mouse) was IV administrated to R-EAE-induced mice on day 9 p.i. R-EAE-induced mice treated with vehicle alone (PBS) or the corresponding isotype control (IC; IgG1 Ab) served as negative controls. The timing of treatment, day 9 p.i., was determined to be the onset day of clinical disability, generally observed in this R-EAE model.

As demonstrated in Fig. 1, R-EAE-induced mice started to develop clinical signs on day 9 post-immunization, and reached to the peak of the first attack on days 11–13, during which the maximal mean score was 2.8 ± 0.2, on day 13, in the IgG1-treated group. IV treatment with anti-BMP-2/4 Ab did not seem to affect the severity of this attack during these days. EAE signs were gradually ameliorated from

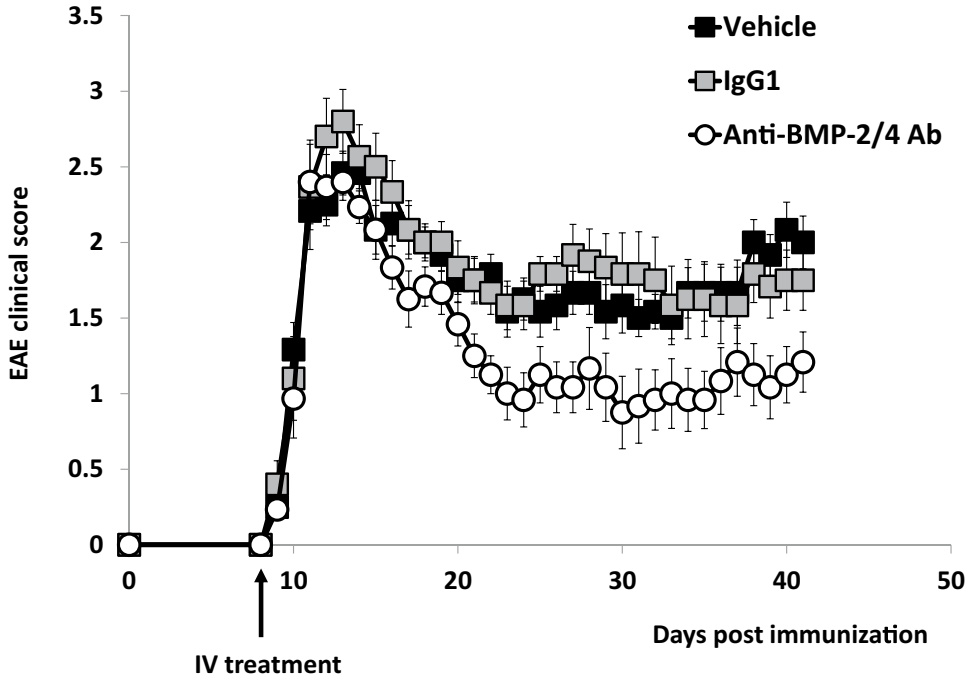

Fig. 1 IV administration of anti-BMP-2/4 mAb ameliorates the clinical signs of R-EAE. Average clinical scores of R-EAE-induced mice that were IV injected, on day 9 p.i., with 30 µg/mouse of either anti-human BMP-2/4 mAb or the corresponding IC (IgG1) or with PBS, which served as the vehicle control group. The minimum number of mice, after sacrifice for pathological assessment, was 12 mice/group. Anti-BMP-2/4 mAb-treated mice exhibited a significant improvement in EAE scores, compared to the IgG1-treated mice, on days 21–27 ($P<0.03$, Mann–Whitney U test), days 29–32 ($P<0.03$), and days 38–40 ($P<0.04$), and compared to the vehicle (PBS)-treated mice, on days 21–27 ($P<0.04$), days 30–32 ($P<0.03$), days 34–35 ($P<0.03$), and days 38–41 ($P\leq0.01$)

day 14 until day 23. A second, more moderate, relapse was observed on days 25–33. From the end of the first attack and on, there was a significant amelioration in the clinical scores of the anti-BMP-2/4 Ab-treated mice, compared to the IgG1-treated mice: on days 21–27 ($P<0.03$, Mann–Whitney U test, per each day scores), days 29–32 ($P<0.03$), and on days 38–40 ($P<0.04$). Anti-BMP-2/4-treated mice also exhibited significant improved signs, compared to the vehicle (PBS)-treated mice, on days 21–27 ($P<0.04$), 30–32 ($P<0.03$), 34–35 ($P<0.03$), and on days 38–41 ($P\leq0.01$).

The clinical EAE characteristics are summarized in Table 1. All R-EAE-induced mice reached, at some point, to a score 1 or above (incidence = 100%). As each of R-EAE-induced mouse reached its' maximal score during the first attack, and treatment with anti-BMP-2/4 Ab did not seem to affect the severity of this attack, no significant differences were observed in the maximum scores, between the anti-BMP-2/4 Ab-treated group (2.8 ± 0.2) and IgG1-treated group (3.4 ± 0.2, $P=NS$), and between the anti-BMP-2/4 Ab-treated group and vehicle-treated group (3.3 ± 0.3, $P=NS$). However, a significant effect of anti-BMP-2/4 Ab treatment on the cumulative scores was observed. The mean of the cumulative scores was 42.9 ± 4.8 in the anti-BMP-2/4-treated group, vs. 57.7 ± 4.3 in the IgG1-treated group (% amelioration = 25.5%, $P=0.03$) and 58.4 ± 2.8 in the vehicle-treated group (% amelioration = 26.4%, $P=0.01$).

Table 1 Clinical characteristics of EAE symptoms

	Vehicle	IgG1	Anti-BMP-2/4 Ab
Incidence (score ≥ 1)	100.0%	100%	100%
Disease onset (days)	9.5 ± 0.2	9.5 ± 0.2	9.6 ± 0.2
Maximum score	3.3 ± 0.3	3.4 ± 0.2	2.8 ± 0.2
Cumulative score	58.4 ± 2.8	57.7 ± 4.3	42.9 ± 4.8

Treatment of R-EAE with Anti-BMP-2/4 mAb Blocks BMP Signaling in the CNS

Phosphorylation of receptor-regulated SMAD1/5/8 is increased upon BMP ligand/receptor interaction and is indicative of BMP pathway activation [59]. In order to evaluate whether the treatment with anti-BMP-2/4 Ab block BMP signaling in the CNS, we next examined the effect of IV treatment with anti-BMP-2/4 mAb on SMAD1/5/8 phosphorylation in the lumbar spinal cord of R-EAE-induced mice. As demonstrated in Fig. 2A, on day 18 p.i., there was around fourfold reduction in the number of phosphorylated-SMAD1/5/8 expressing cells (p-SMAD^{+}/mm^{2}) in the spinal cord of R-EAE-induced mice that were IV treated on day 9 p.i. with

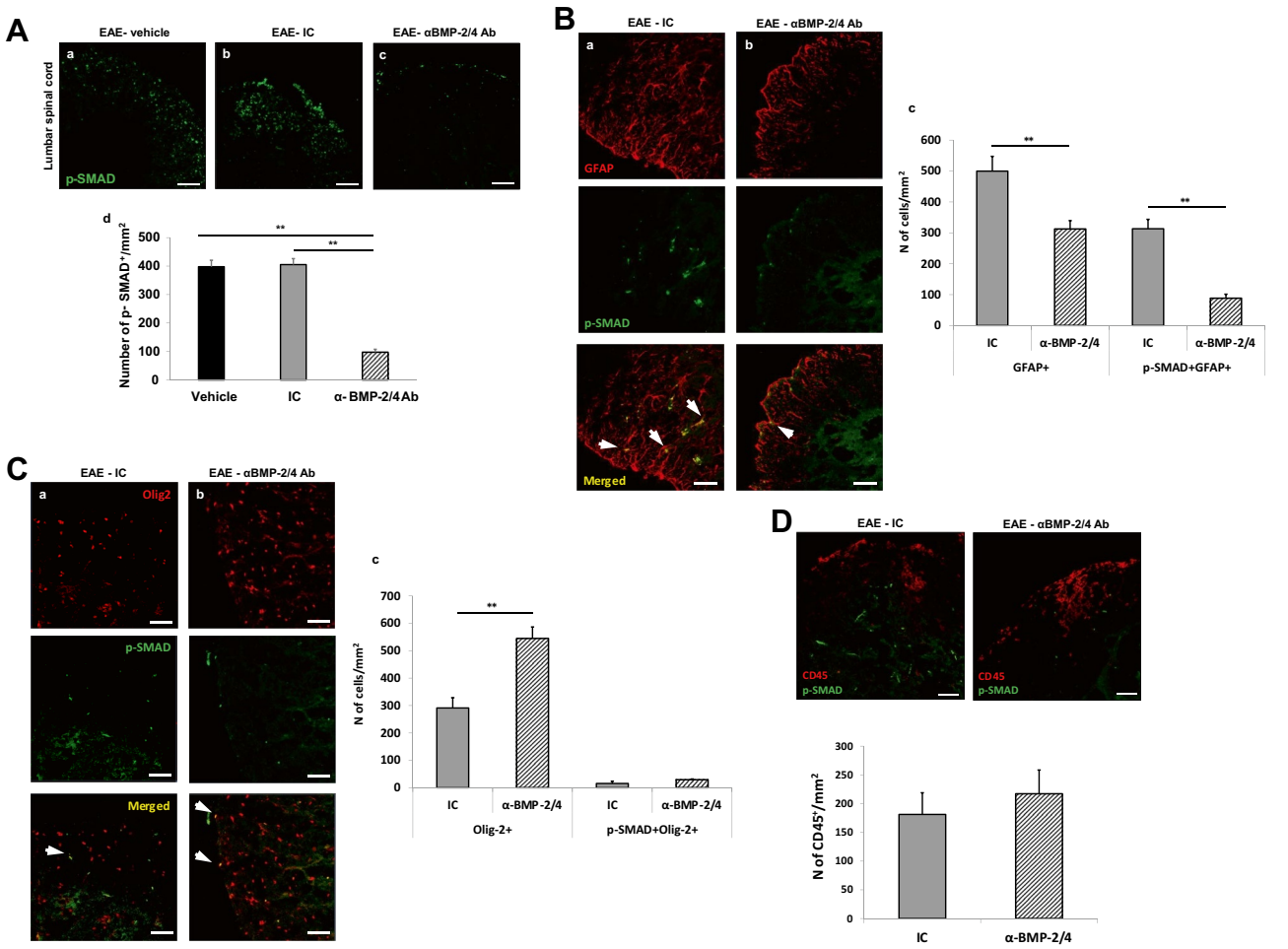

Fig. 2 Reduced numbers of phosphorylated-SMAD1/5/8$^+$cells in the spinal cord of R-EAE mice in response to treatment with anti-BMP-2/4 mAb. **A** Photomicrographs of p-SMAD1/5/8 expressing cells (p-SMAD$^+$) in the lumbar spinal cord (anterior/lateral funiculus) of the vehicle treatment (a), the IC treatment (b), and the anti-BMP-2/4 mAb treatment (c) of R-EAE, on day 18 p.i. Quantification of immunopositive cells showed a decreased phosphorylated-SMAD1/5/8$^+$cells/mm^2 in the anti-BMP-2/4 mAb-treated group vs. both the IC- and the vehicle-treated groups (d). $N=3$ mice/group, scale bar = 50 μm, $^{**}P<0.01$. **B** Co-localization of GFAP and p-SMAD1/5/8 staining demonstrates that most of the p-SMAD$^+$ cells are also GFAP$^+$. Quantification presented in (c) demonstrates reduced numbers of both total GFAP$^+$ cells and double-stained p-SMAD$^+$GFAP$^+$ cells in the anti-BMP-2/4 Ab-treated group (b), compared to the IC-treated group (a), $N=3$ mice/group, scale bar = 50 μm, $^{**}P<0.01$. Arrows indicate double stained cells. **C** Double staining of Olig-2 and p-SMAD1/5/8 in the IC-treated (a) and anti-BMP-2/4 Ab-treated mice reveals negligible numbers of p-SMAD$^+$Olig-2$^+$ cells in both groups. Quantification demonstrates significant elevation in the numbers of total Olig-2$^+$ cells, and no significant differences in the numbers of p-SMAD$^+$Olig-2$^+$ cells (c). $N=3$ mice/group, scale bar = 50 μm, $^{**}P<0.01$. Arrows indicate double stained cells. **D** No co-localization was observed between the p-SMAD1/5/8 and the CD45$^+$ cells in the IC-treated (a) and the anti-BMP-2/4 Ab-treated (b) mice. No significant differences were observed in the numbers of total CD45$^+$ cells (leukocytes) between the groups. $N=3$ mice/group, scale bar = 50 μm

the anti-BMP-2/4 mAb (97.4 ± 10.5 p-SMAD$^+$/mm^2), compared to those that were treated with either IC (405.1 ± 21.2 p-SMAD$^+$/mm^2, $P<0.01$) or with vehicle alone (397.8 ± 22.8 p-SMAD$^+$/mm^2, $P<0.01$), indicating that IV administration of anti-BMP-2/4 mAb reduced the BMP signaling in the disease-affected area of the CNS.

Further analysis of the p-SMAD1/5/8 expressing cells was performed by double staining of p-SMAD1/5/8 with either the GFAP marker, which appear on both astrocytes and NSCs, or Olig-2 (oligodendrocytes), or the CD45 (leukocytes). Overall, we have detected reduced numbers of GFAP$^+$ cells in the anti-BMP-2/4-treated group (312.5 ± 26.9 GFAP$^+$/mm^2), compared to the IC-treated group (499.7 ± 48.0 GFAP$^+$/mm^2, $P<0.01$, Fig. 2B), suggesting that BMP-2/4 blockade reduced astrogliosis or astrogenesis processes. Most of the p-SMAD1/5/8 expressing cells were found to be of GFAP-positive origin in the IC-treated group (77.3%, 313.3 ± 30.5 p-SMAD$^+$GFAP$^+$/mm^2), and treatment with the anti-BMP-2/4 Ab significantly reduced their numbers (88.5 ± 12.9 cells/mm^2, $P<0.01$,

Fig. 2B). The numbers of total Olig-2$^+$ oligodendrocytes were significantly augmented in the anti-BMP-2/4-treated mice (544.9 ± 26.9 Olig-2$^+$/mm^2) compared to the IC-treated group (291.0 ± 37.7 Olig-2$^+$/mm^2, $P < 0.01$, Fig. 2C). However, only 3.8% of the p-SMAD expressing cells were also positive for Olig-2 in the IC-treated group (15.6 ± 7.9 p-SMAD$^+$Olig-2$^+$/mm^2) and their numbers were not significantly altered in response BMP-2/4 blockade (29.3 ± 2.8, P = NS, Fig. 2C).

These findings suggest that treatment with anti-BMP-2/4 Ab mainly affected SMAD signaling in the GFAP$^+$ population. No significant differences were found in the number of CD45$^+$ cells, indicating that the ameliorating effect was probably not mediated via immunosuppression mechanism (IC; 181.2 ± 37.6 CD45$^+$/mm^2, anti-BMP-2/4; 217.2 ± 41.3 CD45$^+$/mm^2, P = NS, Fig. 2D). Moreover, none of the p-SMAD/1/5/8 expressing cells was positive for CD45, indicating that the anti BMP-2/4 did not affect the signaling of p-SMAD in the CNS-infiltrating leukocytes.

Treatment with Anti-BMP-2/4 Ab Promotes Oligodendrocyte Differentiation and Remyelination in R-EAE

Given the clinical advantage of the anti-BMP-2/4 mAb treatment, we studied the effect of this treatment on oligodendrocyte regeneration and remyelination. We daily IP injected 3 mice in each group with BrdU starting from the first day of treatment (day 9) for the next 9 days to detect the de novo differentiation of immature oligodendrocytes (BrdU$^+$Olig-2$^+$PDGFR-α$^+$), mature oligodendrocytes (BrdU$^+$Olig-2$^+$CC1$^+$), and astrocytes (BrdU$^+$GFAP$^+$) in the affected tissue of the lumbar spinal cord [60]. Immunofluorescence staining was performed on lumbar spinal cord tissues harvested from mice on day 18 p.i. As shown in Fig. 3A, there was approximately twofold induction in the number of de novo BrdU$^+$Olig-2$^+$PDGFR-α$^+$immature oligodendrocytes in the lumbar spinal cord in response to anti-BMP-2/4 mAb treatment (177.1 ± 18.6 cells/mm^2 in the anti-BMP-2/4-treated group vs. 88.5 ± 13.3 cells/mm^2 in the IgG1-treated group, $P < 0.01$, Fig. 3A). Furthermore, there was above sevenfold increase, in average, in the number of newly BrdU$^+$Olig-2$^+$CC1$^+$ mature oligodendrocytes in response to anti-BMP-2/4 mAb treatment (190.6 ± 20.5 cells/mm^2) vs. the IC-treated group (25.0 ± 6.1 cells/mm^2, $P < 0.01$, Fig. 3B). Quantification of the percentage of myelin basic protein (MBP)-stained areas, in the lumbar spinal cord, revealed that there was significantly increased myelinated area in the anti-BMP-2/4 mAb-treated EAE mice compared to that in the IC-treated mice (81.0 ± 2.8% in the anti-BMP-2/4-treated group vs. 67.2 ± 3.3% in the IC-treated mice, P = 0.01, Fig. 3C). Moreover, double staining of neurofilament, for axon detection, and fluoromyelin, revealed reduced demyelination and axonal loss in the anti-BMP-2/4-treated mice (fluoromyelin: 77.7 ± 3.2% in the anti-BMP-2/4-treated group vs. 54.4 ± 3.1% in the IC-treated mice, $P < 0.01$ and neurofilament: 98.5 ± 7.1 cells/mm^2 in the anti-BMP-2/4-treated group vs. 64.3 ± 2.5 cells/mm^2 in the IC-treated mice, $P < 0.01$, Fig. 3D).

As BMP signaling is known to induce astrogenesis at the expense of oligodendrogenesis, we have also examined the numbers of de novo BrdU$^+$GFAP$^+$ astrocytes in the lumbar spinal cord. There was a reduction in the number of BrdU$^+$GFAP$^+$ cells in response to treatment with anti BMP-2/4 mAb (7.9 ± 2.9 cells/mm^2) vs. the IC-treated group (77.9 ± 15.1 cells/mm^2, P = 0.008, Fig. 3E). Thus, IV treatment with anti-BMP-2/4 mAb enhances tissue repair by inducing stem cell differentiation into oligodendrocytes concomitant with a reduction in astrogenesis process.

Myelin thickness and structural changes were examined by transmission electron microscopy (TEM, Fig. 4A (a and b)). The scatterplots presented in Fig. 4A (c and d) display g-ratios of individual axons as a function of axon diameter in the IC- and anti-BMP-2/4 Ab-treated R-EAE mice, respectively. The g-ratios in the anti-BMP-2/4 Ab-treated R-EAE mice were lower (average ± S.D = 0.79 ± 0.09) than that of the IC-treated R-EAE mice (0.82 ± 0.10, P = 0.005) and were higher than that of healthy female SJL mice (0.77 ± 0.03, P = 0.001). Axons were categorized into 4 distinct groups (Fig. 4B), as previously described [60]: (i) axons demonstrating g-ratios that are lower than 0.8, which present preexisting myelinated axons (Fig. 4B (a)); (ii) axons with g-ratios between the range of 0.8 and 1, which stand for remyelinated axons (Fig. 4B (b)); (iii) axons with g-ratio = 1, i.e., fully demyelinated axons (Fig. 4B (c)); and (iv) axons exhibiting vesicles within the inner myelin sheath, which represent early myelin fragmentation in EAE, meaning axons that were observed during the process of demyelination (Fig. 4B (d)) [55]. Treatment with anti-BMP-2/4 Ab had no significant effect on the number of preexisting myelinated axons (Fig. 4B (a)). However, this treatment significantly augmented the density of remyelinated axons (Fig. 4B (b), 29.9 ± 4.7 × 10^4 axons/mm^2 in the anti-BMP-2/4-treated EAE vs. 21.1 ± 1.2 × 10^4 axons/mm^2 in IC-treated EAE, $P < 0.01$). Moreover, lower numbers of both fully demyelinated axons (Fig. 4B (c), 12.6 ± 0.7 × 10^4 axons/mm^2) and demyelinating (vesiculated) axons (Fig. 4B (d), 7.7 ± 2.1 × 10^4 axons/mm^2) were observed in the anti-BMP-2/4-treated group, compared to the IC-treated group (19.5 ± 1.1 × 10^4 axons/mm^2 and 17.6 ± 4.8 × 10^4 axons/mm^2, P = 0.02 and $P < 0.01$, respectively), suggesting that BMP-2/4 blockade not only induced the remyelination process, but may also have a myelin protective effect in R-EAE, manifested by reduced demyelinating axons. Overall, in the anti-BMP-2/4 Ab treatment group, 80.2% of the axon were myelinated (premylinated or remyelinated) while in the IC group, 65.0% were myelinated, P = 0.013.

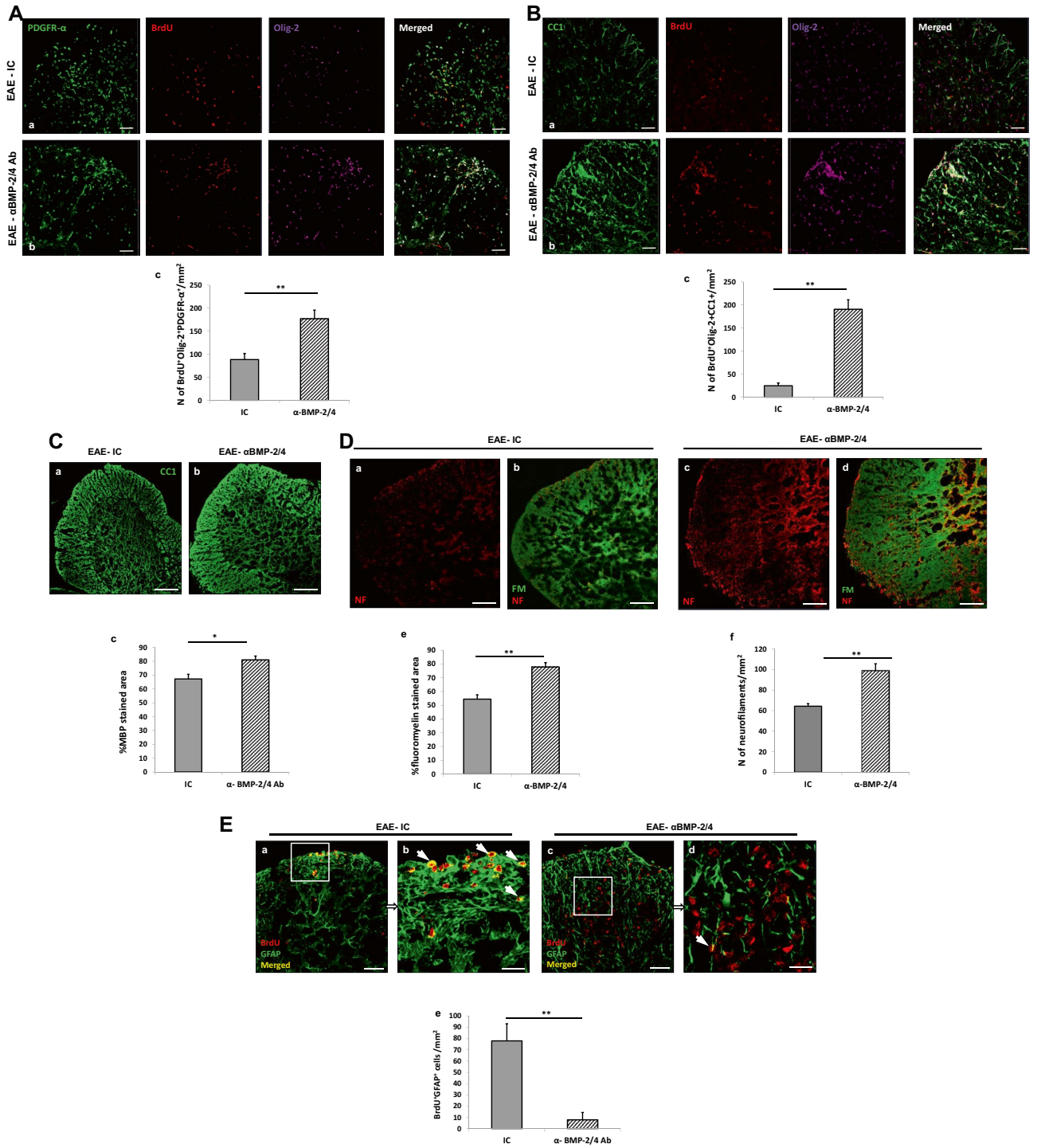

The analysis of the g-ratios according to the axons diameter range (small; 0–1 μm, intermediate; 1–2 μm and large; 2–4 μm) revealed that most of the remyelinated axons were of intermediate size in both the IC- and the anti-BMP-2/4 Ab-treated mice, and the significant induction in the numbers of remyelinated axons was demonstrated among these axons (Fig. 4B (b), $P < 0.05$). Moreover, although most of the fully demyelinated axons were small, with a diameter lower than 1 μm, the reduction in their numbers in response to BMP-2/4 blockade was also primarily observed among the intermediate axons (Fig. 4B (c), $P < 0.01$).

◂**Fig. 3** Increased numbers of newly formed immature and mature oligodendrocytes, concomitant with induced remyelination, are accompanied by reduced numbers of newly generated astrocytes, in the lumbar spinal cords of anti-BMP-2/4-treated mice with R-EAE. Increased numbers of newly generated $BrdU^+Olig\text{-}2^+PDGFR\text{-}\alpha^+$ immature oligodendrocytes **A**, and $BrdU^+Olig\text{-}2^+CC1^+$ mature oligodendrocytes **B** were observed in the lumbar spinal cords of anti-BMP-2/4 mAb-treated R-EAE mice (b), compared to those in IC-treated R-EAE mice (a) on day 18 p.i. The bar graph (c) shows quantification of the triple-positive cells from three mice/group. Scale bar 50 μm; $^{**}P<0.01$. **C** Immunofluorescence staining for MBP in oligodendrocytes in lumbar spinal cords isolated from R-EAE mice treated with IC (a) or with the anti-BMP-2/4 mAb (b), scale bar = 200 μm. The percentage of the myelinated area was increased in anti-BMP-2/4-treated EAE mice (c); $^{*}P<0.05$. **D** Representative cross sections of double staining for fluoromyelin and neurofilament in the IC-treated group (a and b) and in the anti-BMP-2/4-treated group (c and d). Fluoromyelin-stained area increased in the anti-BMP-2/4-treated mice (e), concomitant with reduced loss of neurofilaments, presented in (f). Scale bar = 100 μm; $^{**}P<0.01$. FM fluoromyelin, NF neurofilament. **E** Reduced numbers of $BrdU^+GFAP^+$ astrocytes were observed in the lumbar spinal cords of anti-BMP-2/4 mAb-treated R-EAE mice (c and d) compared with those in IC-treated R-EAE mice (a and b). Quantification of double-positive cells was performed on three mice/group (e). Arrows indicate double-stained cells. The squares marked in a and c are magnified in b and d, respectively. Scale bars: a and c = 50 μm; b and d = 20 μm. $^{**}P<0.01$. $N=3$ mice/group

The Effect of Anti-BMP-2/4 Ab Treatment on Immune Responses in the CNS and in the Periphery

We next examined whether the beneficial clinical effect of treatment with anti-BMP-2/4 neutralizing mAb was also mediated by the suppression of immune responses. We first examined the numbers of $CD45^+$ leukocytes, $CD4^+$ T cells, $CD8^+$ T cells, $CD11b^+$ monocytes, and $CD19^+$ B cells among MNCs isolated from brains and spinal cords on days 14 and 41 p.i. (Table 2, $N=3$ animals per group). We did not detect any significant differences in the levels of any of the immune cell subsets between the anti-BMP-2/4 mAb- and IC-treated groups. Similar findings were observed in the spleen (Tables 3 and 4). Although a trend toward reduced numbers of $CD19^+$ B cells was observed among splenocytes in the anti-BMP-2/4 mAb-treated group compared to those in the IC-treated group on day 14 p.i., this trend was not statistically significant. An examination of the numbers of $CD4^+Foxp3^+$ regulatory T cells, $CD4^+IFN\text{-}\gamma^+$ Th1 cells, $CD4^+IL\text{-}4^+$ Th2 cells, and $CD4^+IL\text{-}17^+$ Th17, also did not reveal a significant immunomodulatory effect in the anti-BMP-2/4 mAb-treated group, compared to the IC-treated group. A nonsignificant trend was observed for the induction of both Th1 and Th2 cells in the spleen in response to BMP-2/4 blockade on day 41 p.i.

Measurement of the proliferation of splenocytes from R-EAE groups in response to T cell stimulation via CD3 or by the cognate peptide proteolipid protein ($PLP_{139\text{-}151}$) at the end of the experiment (day 41), by an XTT proliferation assay ($N=4$ mice per group), did not indicate an immunosuppression mechanism of anti BMP-2/4 mAb. No significant differences were observed in the stimulation ratios (anti-CD3 stimulation/IC stimulation and PLP stimulation/no stimulation) between the group treated with the anti-BMP-2/4 treatment and the IgG1-treated or the vehicle-treated groups (supplementary data, Fig. 2). Hence, overall, we did not detect a significant immunosuppressive/ immunomodulatory effect during the peak of the first relapse, nor at the end of the experiment (day 41).

Treatment with Anti-BMP-2/4 Neutralizing mAb Blocks the BMP Signaling in the CNS and Induces Differentiation into Mature Oligodendrocytes and Remyelination in the Cuprizone Model of Demyelination

We next examined the effect of an IV treatment with anti-BMP-2/4 Ab treatment on oligodendrocyte differentiation and remyelination in the toxic and noninflammatory cuprizone model of demyelination. Mice were fed with cuprizone for 5 weeks (day 35, maximum demyelination) and then transferred to a regular diet. Anti-BMP-2/4 mAb (30 μg/mouse), or the corresponding IC (IgG1), or vehicle alone, were IV administrated on day 15 post-cuprizone diet initiation, as molecular processes of remyelination starts on the third week in this model [62]. Analysis of brain sections was performed 10 days after resuming the regular diet, which is the middle of the recovery phase (day 46).

We first examined whether treatment of cuprizone-fed mice with anti-BMP-2/4 mAb affected BMP signaling in the CNS, as the BBB is known to be less disrupted in this model, in comparison to the EAE. As shown in Fig. 5A, on day 46 (recovery phase), there was a 2.3-fold decrease in the number of $p\text{-}SMAD1/5/8^+$ cells in the medial CC of cuprizone-fed mice which were treated with anti-BMP-2/4 mAb (138.4 ± 22.4 $p\text{-}SMAD^+cells/mm^2$), compared to those that were treated with either IC (324.5 ± 46.2 $p\text{-}SMAD^+cells/mm^2$, $P<0.01$) and to the vehicle-treated mice (321.1 ± 31.3 $p\text{-}SMAD^+cells/mm^2$ in, $P<0.01$).

Similar to the results in the R-EAE model, there were reduced numbers of total GFAP expressing cells, in the anti-BMP-2/4-treated group (341.9 ± 72.4 $GFAP^+/mm^2$), compared to the IC-treated group (665.4 ± 74.8 $GFAP^+/mm^2$, $P<0.05$, Fig. 5B). Moreover, almost all of the $p\text{-}SMAD1/5/8^+$ cells were also positive for the GFAP marker in the IC-treated group (98.4%, 319.6 ± 41.3 $p\text{-}SMAD^+GFAP^+/mm^2$), and treatment with anti-BMP-2/4 Ab significantly decreased their level (136.4 ± 41.9 $cells/mm^2$, $P<0.05$, Fig. 5B). In resemble to the R-EAE model, treatment with anti-BMP-2/4 Ab also increased the density of $Olig\text{-}2^+$ cells in the corpus callosum of cuprizone-fed mice (375.0 ± 55.1 $Olig\text{-}2^+/mm^2$) compared to the IC-treated mice (210.9 ± 21.1 $Olig\text{-}2^+/mm^2$, $P<0.05$, Fig. 5C). However, negligible numbers of $p\text{-}SMAD^+Olig\text{-}2^+$ cells were detected in the

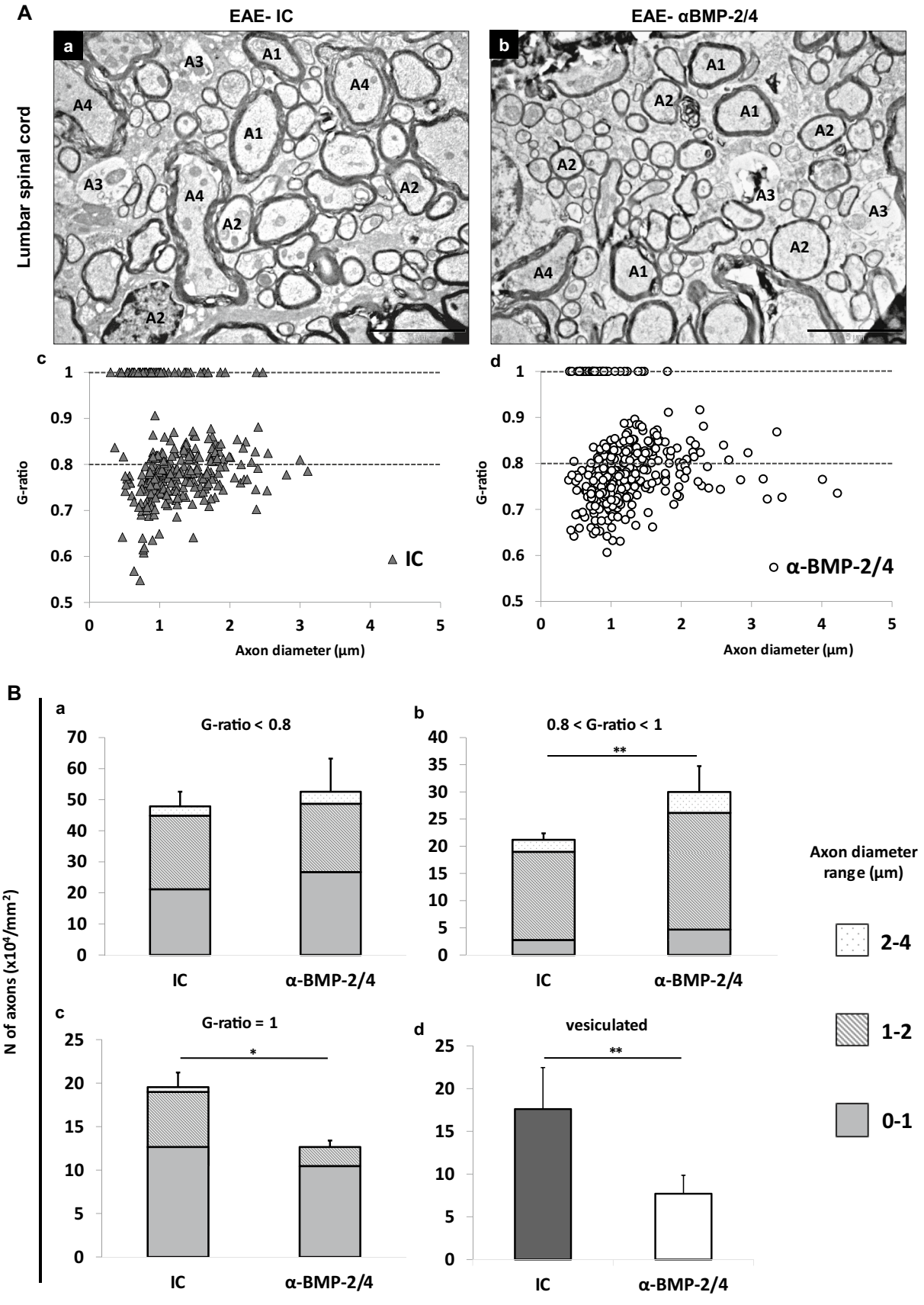
A
EAE- IC
EAE- αBMP-2/4
Lumbar spinal cord
a
b
A1
A2
A3
A4
c
d
G-ratio
Axon diameter (μm)
IC
α-BMP-2/4
B
N of axons (x10⁴/mm²)
G-ratio < 0.8
0.8 < G-ratio < 1
G-ratio = 1
vesiculated
**
*
Axon diameter range (μm)
2-4
1-2
0-1

◂**Fig. 4** Increased remyelination and reduced demyelination in response to BMP-2/4 signaling blockade in R-EAE. **A** Representative electron micrographs of the lumbar spinal cords of IC-treated R-EAE mice (a), and anti-BMP-2/4-treated R-EAE mice (b), on day 18 p.i. Scale bar = 5 µm for both images. Preexisting myelinated axons exhibit g-ratio < 0.8 (A1), whereas remyelinated axons (A2) present thinner myelin sheets (0.8 < g-ratio < 1). Fully demyelinated axons (A3) demonstrate g-ratio = 1, and vesiculated axons, i.e., axons during the demyelination process are marked as A4. The scatterplots display g-ratios of individual axons as a function of axon diameter in IC-treated (c) and anti-BMP-2/4-treated (d) R-EAE mice. **B** Treatment of R-EAE-induced mice with anti-BMP-2/4 Ab did not significantly affect the number of pre-existing myelinated axons, compared to IC (a) but significantly increased the number of remyelinated axons (b) and reduced the number of fully demyelinated axons (c). The bar graphs exhibit the distribution of the axons according to the axon diameter range (small, 0–1 µm; intermediate, 1–2 µm; and large, 2–4 µm). The number of vesiculated axons, i.e., axons that were captured during the process of demyelination, was also significantly reduced in the anti-BMP-2/4 mAb vs. IC-treated R-EAE mice (d). *$P < 0.05$, **$P < 0.01$, chi-squared test, $N = 5$ mice/group, > 200 axons per animal

IC-treated group (7.8 ± 3.6 p-SMAD$^+$Olig-2$^+$/mm^2), which stand for 2.1% of the total p-SMAD expressing cells, and their numbers were not significantly changed in response anti-BMP-2/4 treatment (11.7 ± 1.9, P = NS). As expected, we did not detect CD45-positive cells in the corpus callosum of cuprizone-fed mice in all of the examined groups.

The diminished BMP signaling was accompanied by induction of mature Olig-2$^+$CC1$^+$ oligodendrocytes in the CC (332.5 ± 61.6 cells/mm^2) vs. the IC-treated group (19.0 ± 9.8 cells/mm^2, $P = 0.003$) and vs. the vehicle-treated group (106.6 ± 25.2 cells/mm^2, $P = 0.01$, Fig. 6A). We next examined whether the induced oligodendrocyte differentiation is accompanied with increased remyelination, as detected by MBP staining. After 35 days of feeding the cuprizone diet, cuprizone-challenged mice exhibited a 31.5 ± 2.6% MBP-stained area in the medial CC (Fig. 6B, max demyelination). IV treatment with anti-BMP-2/4 mAb significantly enhanced the myelination of the CC during the recovery phase, on day 46, which is 11 days after returning to the regular diet (87.6 ± 1.8% MBP-stained area) vs. the IC-treated group (66.2 ± 3.6% MBP-stained area, $P < 0.01$) and vs. the vehicle-treated group (46.0 ± 10.5% MBP-stained area, $P < 0.01$, Fig. 6B), indicating that treatment with anti-BMP-2/4 mAb enhances remyelination also in a toxic noninflammatory demyelinating model. Finally, we quantified NF staining in all the examined groups in order to evaluate whether the observed myelin restoration in the anti-BMP-2/4 Ab-treated mice is accompanied with less axonal damage. As demonstrated in Fig. 6C, in compliance to the MBP expression, there was a significant increase in the NF density in response to BMP-2/4 Ab treatment during the recovery phase, indicating a neuroprotective effect of the anti-BMP-2/4 therapy (IC, 60.6 ± 3.2% NF-stained area; anti-BMP-2/4 Ab; 81.8 ± 2.1% NF-stained area, $P < 0.01$).

Discussion

In subjects with MS, BMPs and their receptors are expressed in inflammatory lesions [63], and elevated and deregulated levels of secreted BMPs in the CNS derived from both NSCs [36] and CNS-infiltrating immune cells [48, 64] contribute to the limited differentiation of OPCs and remyelination [12, 30, 34, 35, 37] and to the induction of glial scar formation [44].

Sabo et al. have demonstrated that local blockade of BMP signaling in the CNS, via 14 days of infusion of noggin into the lateral ventricle of cuprizone-fed mice, decreased phosphorylation of SMAD1/5/8, increased the density of mature oligodendrocytes and remyelination in the CC, following 1 week of recovery [40]. Other studies have proposed that, due to its pro-neurogenic properties, noggin may possess therapeutic potential in various neurodegenerative diseases, such as ischemic stroke [65], Parkinson's disease [66], and Alzheimer's disease [67]. Nonetheless, due to the very poor bioavailability of recombinant noggin, with an apparent half-life of less than 60 min, either gene overexpression techniques [65] or continuous intra-CNS delivery systems [40, 41, 67] of noggin, or of the more stabilized format of noggin muteins [53], are often necessary for BMP signaling blockade in the CNS. Moreover, a recent study by Eixarch et al.

Table 2 Number of immune cells in the CNS

Organ	Day post-immunization	Treatment	N CD45 ($\times 10^5$)	N CD4 ($\times 10^5$)	N CD8a ($\times 10^5$)	N CD11b ($\times 10^5$)	N CD19 ($\times 10^5$)
Spinal cord	Day 14	IgG1	1.79 ± 0.44	0.73 ± 0.19	0.16 ± 0.04	0.11 ± 0.03	0.38 ± 0.12
		Anti-BMP-2/4 Ab	1.41 ± 0.43	0.64 ± 0.17	0.11 ± 0.04	0.07 ± 0.02	0.26 ± 0.12
	Day 41	IgG1	2.54 ± 1.14	1.35 ± 0.70	0.36 ± 0.15	0.07 ± 0.02	0.14 ± 0.07
		Anti-BMP-2/4 Ab	2.65 ± 0.67	1.17 ± 0.28	0.41 ± 0.15	0.06 ± 0.01	0.26 ± 0.09
Brain	Day 14	IgG1	2.01 ± 0.45	0.67 ± 0.20	0.17 ± 0.05	0.04 ± 0.01	0.80 ± 0.11
		Anti-BMP-2/4 Ab	2.65 ± 0.25	1.25 ± 0.14	0.23 ± 0.02	0.06 ± 0.01	0.63 ± 0.14
	Day 41	IgG1	1.58 ± 0.91	0.62 ± 0.42	0.18 ± 0.11	0.04 ± 0.01	0.32 ± 0.15
		Anti-BMP-2/4 Ab	1.10 ± 0.49	0.42 ± 0.18	0.17 ± 0.08	0.02 ± 0.01	0.24 ± 0.11

Table 3 Number of immune cells in the spleen

Organ	Day post-immunization	Treatment	N CD45$^+$ ($\times 10^6$)	N CD4$^+$ ($\times 10^6$)	N CD8a$^+$ ($\times 10^6$)	N CD11b$^+$ ($\times 10^6$)	N CD19$^+$ ($\times 10^6$)	N CD4$^+$Foxp3$^+$ ($\times 10^6$)
Spleen	Day 14	IgG1	47.10 ± 3.54	14.05 ± 0.83	6.58 ± 0.41	0.61 ± 0.11	23.53 ± 1.62	1.39 ± 0.13
		Anti-BMP-2/4 Ab	34.57 ± 6.89	12.19 ± 2.21	6.14 ± 1.49	0.48 ± 0.20	14.27 ± 2.81*	1.08 ± 0.28
	Day 41	IgG1	57.08 ± 16.73	17.41 ± 4.83	4.40 ± 0.89	2.37 ± 0.83	30.57 ± 9.62	0.84 ± 0.34
		Anti-BMP-2/4 Ab	56.41 ± 11.23	17.17 ± 3.22	4.38 ± 0.70	2.86 ± 0.41	28.86 ± 7.15	2.55 ± 064

*Trend for CD19$^+$ cells reduction by anti-BMP-2/4 Ab, among splenocytes, $P = 0.06$

has shown that inhibition of the BMP signaling via systemic administration of the small molecule dorsomorphin (DM), or its homologue 1 (DMH1), to MOG-induced EAE mice, ameliorated EAE [68].

Noggin is known to antagonize also BMP-5, BMP-6, BMP-7 [53, 54], growth differentiation factor 5 (GDF-5) [69], and GDF-6 [70], beside BMP-2 and BMP-4, and DM is also a nonspecific BMP receptor antagonist that inhibits the ability of all the BMP type I receptors (ALK1, 2, 3, and 6) to phosphorylate BMP type II receptor [72]. Therefore, and taking into consideration the known association of BMP-2 and BMP-4 with demyelinated pathology [41, 43, 44, 52] and the higher affinity of noggin to BMP-2 and BMP-4, compared to other BMPs [53, 54], the question whether specific inhibition of only BMP-2 and BMP-4 would have a beneficial effect in EAE, and induce oligodendrocyte differentiation and remyelination, remained elusive.

We demonstrate that a single IV administration of anti-BMP-2/4 neutralizing mAb was effective to decrease SMAD1/5/8 phosphorylation in the CNS of both R-EAE and cuprizone models. BBB breakdown is known to occur in R-EAE model, as early as day 6 p.i., before the appearance of the disease signs [71] and in the cuprizone model, as early as 3 days after cuprizone feeding initiation [72], suggesting that it is conceivable that the anti-BMP-2/4 neutralizing Ab penetrated to the CNS when it was administrated on day 9 p.i. to R-EAE mice, or on day 10 post the initiation of the cuprizone feeding. In support with targeting CNS antigen by a mAb in disorders where the blood–CNS barrier is disrupted is the IV treatment with anti-C5 mAb eculizumab in AQP4-positive neuromyelitis optica spectrum disorder that was found to reduce the attack frequency of this disorder [73, 74]. SMAD signaling dysregulation was primarily observed within the GFAP$^+$ cell population, which consists of both NSCs and astrocytes. This finding suggests that the alleviating effect of anti-BMP-2/4 Ab treatment could be mediated either via reduced SMAD signaling within the NSCs, leading these cells to undergo differentiation toward the oligodendrocyte lineage, or by inhibition of the astrogliosis process, which has been demonstrated to be associated with remyelination [44].

Indeed, the specific blockade of BMP-2 and BMP-4 signaling by systemic mAb treatment approach, in the noninflammatory cuprizone model of demyelination, augmented the numbers of mature oligodendrocytes and remyelination, as well as the density of surviving axons, in the CC, during the recovery phase of the disease, indicating that this clinically applicable approach induces oligodendrocyte regeneration, remyelination, and neuroprotection.

Moreover, IV injection of the anti-BMP-2/4 mAb to R-EAE-induced mice, ameliorated EAE signs following the first attack, during days 23–41. The lack of a significant effect during the first attack implies that the alleviating effect was probably mainly mediated by time-consuming processes, such as OPC differentiation and remyelination, as was demonstrated later on. Similar postponed ameliorating effects were observed in response to other optional pro-remyelinating therapies, such as kappa opioid receptor (KOR) agonists [75] and clemastine, in which the first significant alleviation was observed on day 18 p.i. in the MOG-induced chronic EAE model [61].

Table 4 Th1, Th2, and Th17 cell distribution among CD4 + splenocytes post-stimulation

Organ	Day post-immunization	Treatment	%IFN-γ$^+$ of CD4$^+$	%IL-4$^+$ of CD4$^+$	%IL-17$^+$ of CD4$^+$
Spleen	Day 14	IgG1	4.64 ± 1.86	2.54 ± 0.78	1.58 ± 0.71
		Anti-BMP-2/4 Ab	4.34 ± 0.99	2.63 ± 0.64	0.97 ± 0.38
	Day 41	IgG1	4.25 ± 0.87	2.63 ± 0.38	1.28 ± 0.28
		Anti-BMP-2/4 Ab	7.57 ± 1.05*	3.88 ± 0.25**	1.73 ± 0.26

*Trend for induction in %IFN-γ$^+$ of CD4 + cells, by anti-BMP-2/4 Ab, $P = 0.07$

**Trend for induction in %IL-4$^+$ of CD4 + cells, by anti-BMP-2/4 Ab, $P = 0.06$

Indeed, histopathological examination of the lumbar spinal cord of R-EAE-induced mice revealed increased numbers of de novo immature ($BrdU^+Olig\text{-}2^+PDGFR\text{-}\alpha^+$) and mature oligodendrocytes ($BrdU^+Olig\text{-}2^+CC1^+$), as well as reduced $BrdU^+GFAP^+$ astrocytes, indicating that this treatment favored NSCs or OPCs differentiation to mature oligodendrocytes at the expense of astrogenesis processes within the affected spinal cord of R-EAE. This effect was noticed as early as 9 days after therapy installment.

Induced differentiation of OPCs to mature oligodendrocytes, in response to BMP-2/4 blockade in R-EAE, was accompanied with enhanced remyelination, as reflected by increased MBP and fluromyelin staining, and augmented numbers of remyelinated axons exhibiting g-ratios in the range between 0.8 and 1, which was mostly evident among the intermediate size axons. The reduced numbers of fully demyelinated axons in the anti-BMP-2/4-treated mice supports the notion that accelerated remyelination during inflammatory demyelination attenuates the demyelination

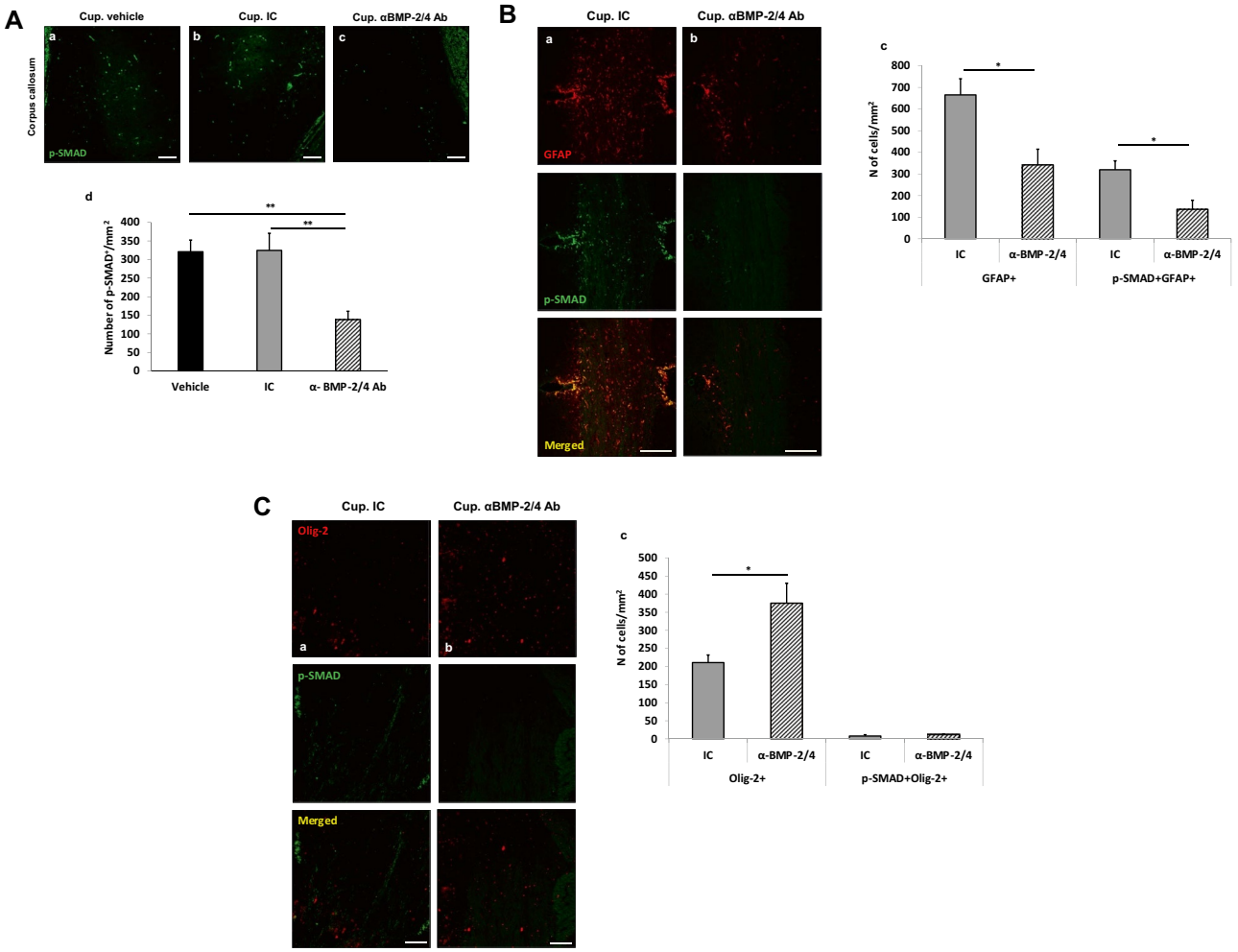

Fig. 5 IV administration of anti-BMP-2/4 mAb decreases phosphorylation of SMAD1/5/8, induces mature oligodendrocytes and remyelination in the corpus callosum of cuprizone toxic model of demyelination. C57BL/6 male mice were fed 0.2% cuprizone for 35 days and then transferred to a regular diet. The anti-BMP-2/4 neutralizing mAb was IV administered (30 µg/mouse) on day 15 after initiation of the cuprizone diet. The control group was IV injected with 30 µg/mouse of the corresponding IC, mouse IgG1. Immunohistochemical analysis of the medial CC was performed on day 46, 11 days after cuprizone withdrawal, during the recovery phase ($N=5$ mice/group). **A** Reduced numbers of p-SMAD1/5/8$^+$ cells in the CC of anti-BMP-2/4 mAb-treated mice (c), compared to both IC-treated mice (b), and vehicle-treated mice (a), scale bar = 50 µm. Quantification of p-SMAD1/5/8$^+$ cells/mm^2 is presented in (d), $^{**}P<0.01$. **B** Double staining of GFAP and p-SMAD1/5/8 shows that almost all of the p-SMAD$^+$ cells are GFAP-positive. Quantification exhibited in (c) demonstrates reduced numbers of GFAP$^+$ cells and p-SMAD$^+$GFAP$^+$ cells in the anti-BMP-2/4 Ab-treated group (b), compared to the IC-treated group (a), $N=3$ mice/group, scale bar = 100 µm, $^*P<0.05$. **C** Co-localization of Olig-2 and p-SMAD1/5/8 in the IC-treated (a) and anti-BMP-2/4 Ab-treated mice shows that the numbers of p-SMAD$^+$Olig-2$^+$ cells are infrequent in both groups. There was a significant increase in the numbers of total Olig-2$^+$ cells, but no significant differences in the numbers of the double-stained cells (c). $N=3$ mice/group, scale bar = 50 µm, $^*P<0.05$

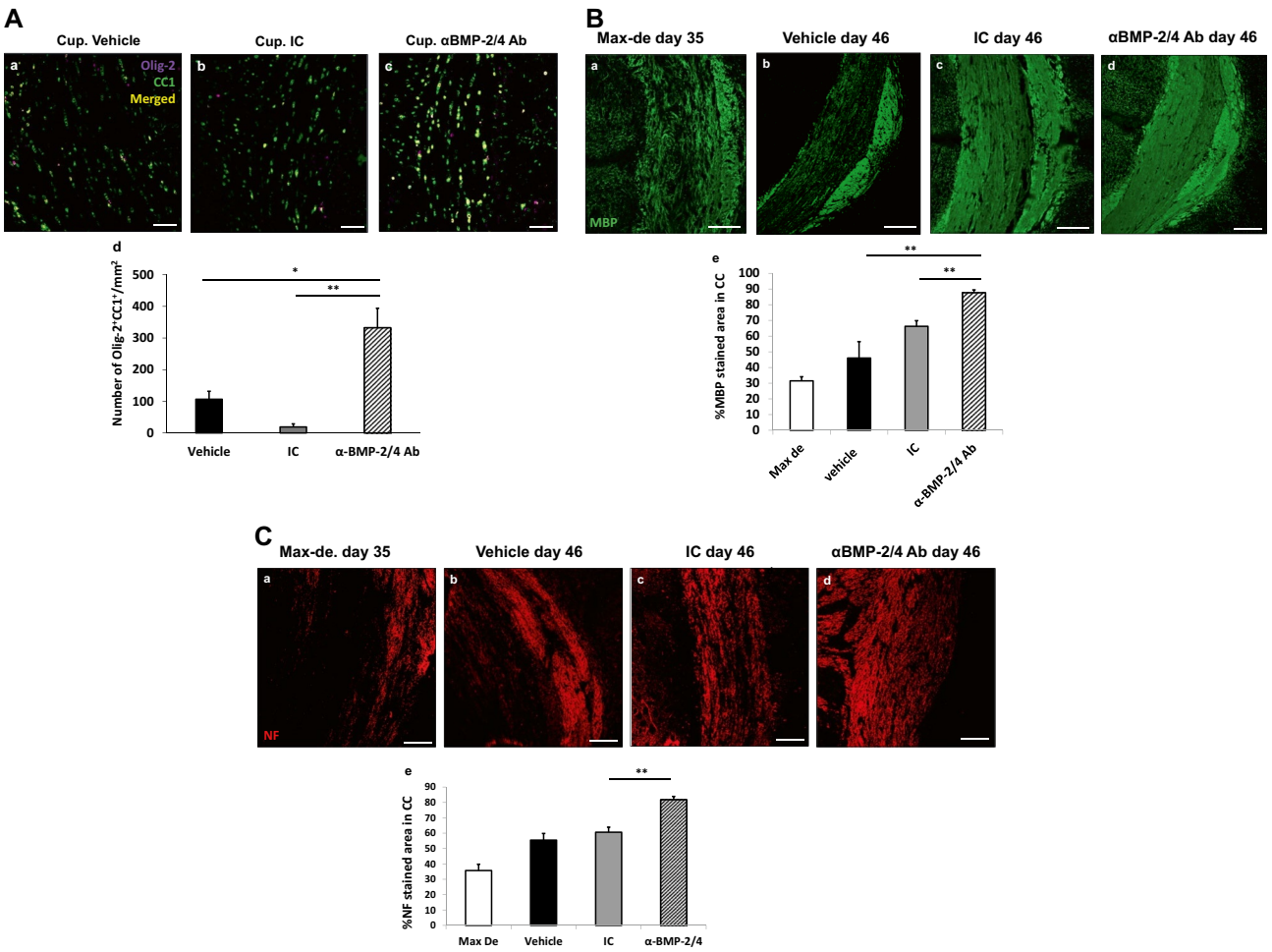

Fig. 6 Anti-BMP-2/4 mAb treatment increases the numbers of mature oligodendrocytes, the density of the myelinated area and of neurofilaments in the corpus callosum of cuprizone toxic model of demyelination. **A** Immunofluorescence staining for mature Olig-2^+CC1^+ oligodendrocytes on day 46 revealed increased numbers of Olig-2^+CC1^+ oligodendrocytes in the medial CC of anti-BMP-2/4 mAb-treated mice (c) compared to that in IC-treated (b) and in vehicle-treated (a) mice. The bar graph (d) shows a summary of the results from the 5 tested animals in each group. Scale bar = 50 μm, $^*P < 0.05$, $^{**}P < 0.01$. **B** The medial CC is extensively demyelinated after 35 days of cuprizone diet (a). An increased percentage of the MBP-stained area was observed in the anti-BMP-2/4 treated group (d) compared to that in the IC-treated group (c) and to that of the vehicle-treated group (b), on day 46. Quantification of the results from the 5 tested animals in each group is presented in the bar graph (d). Scale bar = 100 μm, $^{**}P < 0.01$. **C** Neurofilament density was substantially reduced after 35 days of cuprizone diet (a). Neurofilament-stained area was enhanced in the anti-BMP-2/4-treated group (d) compared to that in the IC-treated group (c) during the recovery phase. Quantification is shown in the bar graph (d). $N = 5$ in each group. Scale bar = 50 μm, $^{**}P < 0.01$. NF neurofilament

process, as was demonstrated in EAE induced in *Chrm1 fl/fl* mice, in which the target of clemasine; the muscarinic receptor, was conditional knocked-out [61]. Moreover, it has been previously demonstrated that myelin vesiculation, i.e., the appearance of myelin sheaths with signs of vesicular disruption, is a major pattern of early myelin fragmentation in the spinal cords of EAE induced in Biozzi mice [56]. We have observed a reduced number of vesiculated axons in the anti-BMP-2/4 mAb-treated mice, indicating that this treatment also attenuated myelin pathology deterioration. These findings suggest that BMP-2/4 blockade not only induces repair processes, but may also have an oligodendrocyte- and myelin-protective effect. Such an effect has been previously demonstrated, as exposure of oligodendroglial cells to conditioned media from noggin-treated reactive microglia, during oxygen/glucose deprivation and reperfusion, reduced the oligodendroglia death [76].

Furthermore, we have directly approached the question whether the beneficial effect of anti-BMP-2/4 mAb in R-EAE was also mediated by suppression of the immune responses. Immune cells not only express BMPs but may also respond to BMP stimulation [77–80]. However, controversy exists regarding whether BMPs exert a pro- or anti-inflammatory effect. Stimulation of naïve $CD4^+$ T cells

with TGF-β in the presence of BMP-2/4 enhances the differentiation and suppressive activity of regulatory T cells (Tregs) [79], and the activation of $CD4^+$ T cells with defective BMPR1α results in increased IFN-γ production and increased cell proliferation, supporting anti-inflammatory effects of BMPs [78]. In contrast, the inhibition of BMP signaling with DM impairs T cell proliferation by reducing IL-2 production [81], and BMP-4 was found to induce IFN-γ production in $CD8^+$ T cells upon antigen stimulation [82], indicating a proinflammatory role of BMPs. We did not detect a significant effect of the anti-BMP-2/4 mAb on the number of CD45 + cells in the affected tissue in the spinal cord, on the numbers of $CD4^+$ T cells, $CD8^+$ T cells, monocytes, or B cells among MNCs of the brains, spinal cords, or splenocytes at the peak of the first attack (day 14 p.i.) or on day 41 p.i.. No significant effects of the BMP-2/4 blockade were observed on the Th1, Th2, Th17, or Treg populations in the spleen. Moreover, we did not observe an effect on the proliferation of spleen-derived T cells in response to stimulation with anti CD3 or with $PLP_{139\text{-}151}$ in the R-EAE group treated with anti-BMP-2/4 mAb.

Eixarch et al. studied the immunological effect of DMH1 in EAE and showed that this treatment was associated with a reduction in the overall myeloid population in splenocytes, with an increased frequency of plasmacytoid dendritic cells and a reduced M2 macrophages population [68] which resulted, at least in part, by the blockade of BMP-6 and BMP-7 activity [83–87]. In similar to our findings, they did not find a significant effect of DMH1 on Th1, Th2, Th17, Treg, and M2 macrophages in the spinal cord and on T- and B-cell subsets in the peripheral immune system. In light of their research, there is also an immunosuppressive effect of the BMP receptor blockade, which is probably depended on the inhibition of BMPs that are different form BMP-2 and BMP-4. Our study that showed oligodendrocyte regeneration and remyelination effects of BMP-2/4 blockade did not completely rule out any immunological effect of this therapy, as we did not study the function of immune cells subsets.

In conclusion, a specific blockade of BMP-2/4 signaling, via a single IV administration of anti-BMP2/4 mAb, exhibits an oligodendrocyte regenerative and a remyelinating effect in both inflammatory and noninflammatory demyelinating diseases of the CNS. Herein, treatment with anti-BMP-2/4 mAb has the potential to become a therapeutic approach for oligodendrogenesis and myelin repair in patients with demyelinating disease such as MS. The existing therapies for MS affect mainly the immune mechanism of the disease, and there is no approved therapy for myelin repair. It is therefore suggested that the treatment with anti-BMP2/4 mAb could potentially be combined with immune-targeted therapy for MS.

Supplementary Information The online version contains supplementary material available at https://doi.org/10.1007/s13311-021-01068-9.

Required Author Forms Disclosure forms provided by the authors are available with the online version of this article.

Funding The study was supported in part by the Israel Scientific Foundation—Grant #1022/10.

References

1. Barnett MH, Prineas JW. Relapsing and Remitting Multiple Sclerosis: Pathology of the Newly Forming Lesion. Ann Neurol. 2004; 5: 458-68.
2. Prat A, Antel J. Pathogenesis of multiple sclerosis. Curr Opin Neurol. 2005;18: 225-230.
3. Matute C, Pérez-Cerdá F. Multiple sclerosis: Novel perspectives on newly forming lesions. Trends Neurosci. 2005; 28: 173-175.
4. Frohman EM, Racke MK, Raine CS. Multiple Sclerosis — The Plaque and Its Pathogenesis. N Engl J Med. 2006; 354: 942–955.
5. Trapp BD, Nave K-A. Multiple Sclerosis: An Immune or Neurodegenerative Disorder? Annu Rev Neurosci. 2008; 31: 247–269.
6. Dendrou CA, Fugger L, Friese MA. Immunopathology of multiple sclerosis. Nat Rev Immunol. 2015; 15: 545-558.
7. Stankoff B, Jadasz JJ, Hartung H-P, et al. Repair strategies for multiple sclerosis: challenges, achievements and perspectives. Curr Opin Neurol. 2016; 29: 286–292.
8. Kornek B, Storch MK, Weissert R, et al. Multiple sclerosis and chronic autoimmune encephalomyelitis: a comparative quantitative study of axonal injury in active, inactive, and remyelinated lesions. Am J Pathol. 2000; 157: 267–276.
9. Irvine KA, Blakemore WF. Remyelination protects axons from demyelination-associated axon degeneration. Brain. 2008; 131: 1464–1477.
10. Bruce CC, Zhao C, Franklin RJM. Remyelination - An effective means of neuroprotection. Horm Behav. 2010; 57: 56–62.
11. Wolswijk G. Chronic Stage Multiple Sclerosis Lesions Contain a Relatively Quiescent Population of Oligodendrocyte Precursor Cells. J Neurosci. 1998; 18: 601-9.
12. Lucchinetti C, Bruck W, Parisi J, et al. A quantitative analysis of oligodendrocytes in multiple sclerosis lesions. A study of 113 cases. Brain. 1999; 122 (Pt 12): 2279–2295.
13. Maeda Y, Solanky M, Menonna J, et al. Platelet-derived growth factor-alpha receptor-positive oligodendroglia are frequent in multiple sclerosis lesions. Ann Neurol. 2001; 49: 776–785.
14. Chang A, Tourtellotte WW, Rudick R, et al. Premyelinating Oligodendrocytes in Chronic Lesions of Multiple Sclerosis. N Engl J Med. 2002; 346: 165-73.
15. Nait-Oumesmar B, Picard-Riera N, Kerninon C, et al. Activation of the subventricular zone in multiple sclerosis: evidence for early glial progenitors. Proc Natl Acad Sci U S A. 2007;104:4694–4699.
16. Snethen H, Love S, Scolding NJ. Disease-responsive neural precursor cells are present in multiple sclerosis lesions. Regen Med. 2008; 3: 835-47.
17. Nait-Oumesmar B, Decker L, Lachapelle F, et al. Progenitor cells of the adult mouse subventricular zone proliferate, migrate and differentiate into oligodendrocytes after demyelination. Eur J Neurosci. 1999; 11: 4357–4366.
18. Aguirre A, Dupree JL, Mangin JM, et al. A functional role for EGFR signaling in myelination and remyelination. Nat Neurosci. 2007; 10: 990–1002.
19. Patel JR, McCandless EE, Dorsey D, et al. CXCR4 promotes differentiation of oligodendrocyte progenitors and remyelination. Proc Natl Acad Sci U S A. 2010; 107: 11062–11067.

20. Samanta J, Grund EM, Silva HM, et al. Inhibition of Gli1 mobilizes endogenous neural stem cells for remyelination. Nature. 2015; 526: 448–452.
21. Mi S, Lee X, Hu Y, et al. Death receptor 6 negatively regulates oligodendrocyte survival, maturation and myelination. Nat Med. 2011; 17: 816–821.
22. Perier O, Gregoire A. Electron microscopic features of multiple sclerosis lesions. Brain. 1965; 88: 937–952.
23. Prineas JW, Connell F. Remyelination in multiple sclerosis. Ann Neurol. 1979; 5: 22–31.
24. Raine CS, Wu E. Multiple sclerosis: remyelination in acute lesions. J Neuropathol Exp Neurol. 1993; 52: 199–204.
25. Patrikios P, Stadelmann C, Kutzelnigg A, et al. Remyelination is extensive in a subset of multiple sclerosis patients. Brain. 2006; 129: 3165–3172.
26. Patani R, Balaratnam M, Vora A, et al. Remyelination can be extensive in multiple sclerosis despite a long disease course. Neuropathol Appl Neurobiol. 2007; 33: 277-87.
27. Kotter MR, Li W-W, Zhao C, et al. Myelin Impairs CNS Remyelination by Inhibiting Oligodendrocyte Precursor Cell Differentiation. J Neurosci. 2006; 26: 328–332.
28. Miller RH, Mi S. Dissecting demyelination. Nat Neurosci. 2007; 10: 1351–1354.
29. Piaton G, Aigrot M-S, Williams A, et al. Class 3 semaphorins influence oligodendrocyte precursor recruitment and remyelination in adult central nervous system. Brain. 2011; 134: 1156–1167.
30. Kuhlmann T, Miron V, Cuo Q, et al. Differentiation block of oligodendroglial progenitor cells as a cause for remyelination failure in chronic multiple sclerosis. Brain. 2008; 131(Pt 7):1749-58.
31. Lucchinetti CF, Bruck W, Rodriguez M, et al. Distinct patterns of multiple sclerosis pathology indicates heterogeneity on pathogenesis. Brain Pathol. 1996; 6: 259–274.
32. Correale J, Farez MF. The role of astrocytes in multiple sclerosis progression. Front Neurol. 2015; 6: 1–12.
33. Gross RE, Mehler MF, Mabie PC, et al. Bone morphogenetic proteins promote astroglial lineage commitment by mammalian subventricular zone progenitor cells. Neuron. 1996; 17: 595-606.
34. Mabie PC, Mehler MF, Marmur R, et al. Bone morphogenetic proteins induce astroglial differentiation of oligodendroglial-astroglial progenitor cells. J Neurosci. 1997; 17: 4112-20.
35. Grinspan J, Edell E, Carpio DF, et al. Stage-specific effects of bone morphogenetic proteins on the oligodendrocyte lineage. J Neurobiol. 2000; 43: 1–17.
36. Lim DA, Tramontin AD, Trevejo JM, et al. Noggin antagonizes BMP signaling to create a niche for adult neurogenesis. Neuron. 2000; 28: 713-26.
37. Gomes WA, Mehler MF, Kessler JA. Transgenic overexpression of BMP4 increases astroglial and decreases oligodendroglial lineage commitment. Dev Biol. 2003; 255: 167-7.
38. Colak D, Mori T, Brill MS, et al. Adult Neurogenesis Requires Smad4-Mediated Bone Morphogenic Protein Signaling in Stem Cells. J Neurosci. 2008; 28: 434–446.
39. Sabo JK, Kilpatrick TJ, Cate HS. Effects of Bone Morphogenic Proteins on Neural Precursor Cells and Regulation during Central Nervous System Injury. Neurosignals. 2009; 17: 255–264.
40. Sabo JK, Aumann TD, Merlo D, et al. Remyelination Is Altered by Bone Morphogenic Protein Signaling in Demyelinated Lesions. J Neurosci. 2011; 31: 4504-10.
41. Cate HS, Sabo JK, Merlo D, et al. Modulation of bone morphogenic protein signalling alters numbers of astrocytes and oligodendroglia in the subventricular zone during cuprizone-induced demyelination. J Neurochem. 2010; 115: 11-22.
42. Jablonska B, Aguirre A, Raymond M, et al. Chordin-induced lineage plasticity of adult SVZ neuroblasts after demyelination. Nat Neurosci. 2010; 13: 541–550.
43. Zhao C, Fancy SPJ, Magy L, et al. Stem cells, progenitors and myelin repair. J. Anat. 2005; 207: 251-8.
44. Fuller ML, DeChant AK, Rothstein B, et al. Bone morphogenetic proteins promote gliosis in demyelinating spinal cord lesions. Ann Neurol. 2007; 62: 288-300.
45. Ara J, See J, Mamontov P, et al. Bone Morphogenetic Proteins 4, 6, and 7 Are Up-Regulated in Mouse Spinal Cord during Experimental Autoimmune Encephalomyelitis. J Neurosci Res 2008; 86: 125-35.
46. Deininger M, Meyermann R, Schluesener H. Detection of two transforming growth factor-$β$-related morphogens, bone morphogenetic proteins-4 and-5, in RNA of multiple sclerosis and Creutzfeldt-Jakob disease lesions. Acta Neuropathol. 1995; 90: 76–79.
47. Costa C, Eixarch H, Martínez-Sáez E, et al. Expression of Bone Morphogenetic Proteins in Multiple Sclerosis Lesions. Am J Pathol. 2019; 189: 665–676.
48. Mausner-Fainberg K, Urshansky N, Regev K, et al. Elevated and dysregulated bone morphogenic proteins in immune cells of patients with relapsing-remitting multiple sclerosis. J Neuroimmunol. 2013; 264: 91-99.
49. Urshansky N, Mausner-Fainberg K, Auriel E, et al. Reduced production of noggin by immune cells of patients with relapsing-remitting multiple sclerosis. J Neuroimmunol. 2011; 232: 171-178.
50. Urshansky N, Mausner-Fainberg K, Auriel E, et al. Low and dysregulated production of follistatin in immune cells of relapsing-remitting multiple sclerosis patients. J Neuroimmunol. 2011; 238: 96-103.
51. Penn M, Mausner-Fainberg K, Golan M, et al. High serum levels of BMP-2 correlate with BMP-4 and BMP-5 levels and induce reduced neuronal phenotype in patients with relapsing-remitting multiple sclerosis. J Neuroimmunol. 2017; 310: 120-128.
52. Cheng X, Wang Y, He Q, et al. Bone morphogenetic protein signaling and olig1/2 interact to regulate the differentiation and maturation of adult oligodendrocyte precursor cells. Stem Cells. 2007; 25: 3204–3214.
53. Aspenberg P, Jeppsson C, Economides AN. The Bone Morphogenetic Proteins Antagonist Noggin Inhibits Membranous Ossification. J Bone Miner Res. 2001; 16: 497–500.
54. Groppe J, Greenwald J, Wiater E, et al. Structural basis of BMP signalling inhibition by the cystine knot protein Noggin. Nature. 2002; 420: 636–642.
55. Yang J, Shi P, Tu M, et al. Bone morphogenetic proteins: Relationship between molecular structure and their osteogenic activity. Food Sci Hum Wellness. 2014; 3: 127-135.
56. Weil M-T, Mobius W, Winkler A, et al. Loss of Myelin Basic Protein Function Triggers Myelin Breakdown in Models of Demyelinating Diseases. Cell Rep. 2016; 16: 314–322.
57. Pino PA, Cardona AE. Isolation of brain and spinal cord mononuclear cells using percoll gradients. J Vis Exp. 2011; 48: 2348.
58. Bani-Yaghoub M, Felker JM, Sans C, et al. The Effects of Bone Morphogenetic Protein 2 and 4 (BMP2 and BMP4) on Gap Junctions during Neurodevelopment. Exp Neurol. 2000; 162: 13–26.
59. Massague J. TGF-beta signal transduction. Annu Rev Biochem. 1998; 67: 753–791.
60. Fu Y, Frederick TJ, Huff TB, et al. Paranodal myelin retraction in relapsing experimental autoimmune encephalomyelitis visualized by coherent anti-Stokes Raman scattering microscopy. J Biomed Opt. 2011; 16: 106006.
61. Mei F, Lehmann-Horn K, Shen Y-AA, et al. Accelerated remyelination during inflammatory demyelination prevents axonal loss and improves functional recovery. Elife. 2016; 5: e18246.
62. Kipp M, Clarner T, Dang J, et al. The cuprizone animal model: New insights into an old story. Acta Neuropathol. 2009; 118: 723–736.

63. Costa C, Eixarch H, Martinez-Saez E, et al. Expression of Bone Morphogenetic Proteins in Multiple Sclerosis Lesions. Am J Pathol. 2018; 189: 665-676.
64. Teresa C, Rosa S, Carmen H-L, et al. Bone morphogenetic protein-2/4 signalling pathway components are expressed in the human thymus and inhibit early T-cell development. Immunology. 2007; 121: 94–104.
65. Samanta J, Alden T, Gobeske K, et al. Noggin Protects against Ischemic Brain Injury in Rodents. Stroke. 2010; 41: 357-362.
66. Shunmei C, Mook LY, Wenbo Z, et al. Noggin Enhances Dopamine Neuron Production from Human Embryonic Stem Cells and Improves Behavioral Outcome After Transplantation into Parkinsonian Rats. Stem Cells. 2008; 26: 2810–2820.
67. Tang J, Song M, Wang Y, et al. Noggin and BMP4 co-modulate adult hippocampal neurogenesis in the APPswe/PS1ΔE9 transgenic mouse model of Alzheimer's disease. Biochem Biophys Res Commun. 2009; 385: 341–345.
68. Eixarch H, Calvo-Barreiro L, Costa C, et al. Inhibition of the BMP Signaling Pathway Ameliorated Established Clinical Symptoms of Experimental Autoimmune Encephalomyelitis. Neurotherapeutics 2020; 17: 1988-2003.
69. Merino R, Macias D, Gañan Y, et al. Expression and Function of GDF-5 during Digit Skeletogenesis in the Embryonic Chick Leg Bud. Dev Biol. 1999; 206: 33–45.
70. Chang C, Hemmati-Brivanlou A. Xenopus GDF6, a new antagonist of noggin and a partner of BMPs. Development. 1999; 126: 3347–3357.
71. Tonra JR, Reiseter BS, Kolbeck R, et al. Comparison of the timing of acute blood-brain barrier breakdown to rabbit immunoglobulin G in the cerebellum and spinal cord of mice with experimental autoimmune encephalomyelitis. J Comp Neurol. 2001; 430: 131–144.
72. Berghoff SA, Duking T, Spieth L, et al. Blood-brain barrier hyperpermeability precedes demyelination in the cuprizone model. Acta Neuropathol Commun. 2017; 5: 94.
73. Pittock SJ, Lennon VA, McKeon A, et al. Eculizumab in AQP4-IgG-positive relapsing neuromyelitis optica spectrum disorders: an open-label pilot study. Lancet Neurol. 2013; 12: 554–562.
74. Carpanini SM, Torvell M, Morgan BP. Therapeutic Inhibition of the Complement System in Diseases of the Central Nervous System. Front Immunol. 2019;10:362.
75. Du C, Duan Y, Wei W, et al. Kappa opioid receptor activation alleviates experimental autoimmune encephalomyelitis and promotes oligodendrocyte-mediated remyelination. Nat Commun. 2016; 7: 11120.
76. Shin JA, Kim YA, Kim HW, et al. Iron released from reactive microglia by noggin improves myelin repair in the ischemic brain. Neuropharmacology. 2018; 133: 202–215.
77. Eixarch H, Calvo-Barreiro L, Montalban X, et al. Bone morphogenetic proteins in multiple sclerosis: Role in neuroinflammation. Brain Behav Immun. 2018; 68: 1–10.
78. Kuczma M, Kurczewska A, Kraj P. Modulation of Bone Morphogenic Protein Signaling in T-Cells for Cancer Immunotherapy. J Immunotoxicol. 2014; 11: 319–327.
79. Ling L, Jilin M, Xuehao W, et al. Synergistic effect of TGF-β superfamily members on the induction of Foxp3+ Treg. Eur J Immunol. 2009; 40: 142–152.
80. Yumiko Y, Masahiro O, Motonao O, et al. Differential effects of inhibition of bone morphogenic protein (BMP) signalling on T-cell activation and differentiation. Eur J Immunol. 2012; 42: 749–759.
81. Martínez VG, Sacedón R, Hidalgo L, et al. The BMP Pathway Participates in Human Naive CD4(+) T Cell Activation and Homeostasis. Houtman JCD, editor. PLoS One. 2015; 10: e0131453.
82. Takai S, Tokuda H, Matsushima-Nishiwaki R, et al. TGF-beta superfamily enhances the antigen-induced IFN-gamma production by effector/memory CD8+ T cells. Int. J. Mol. Med. 2010; 25: 105-11.
83. Lee GT, Kwon SJ, Lee J-H, et al. Induction of interleukin-6 expression by bone morphogenetic protein-6 in macrophages requires both SMAD and p38 signaling pathways. J Biol Chem. 2010; 285: 39401–39408.
84. Hong JH, Lee GT, Lee JH, et al. Effect of bone morphogenetic protein-6 on macrophages. Immunology. 2009; 128: e442-50.
85. Kwon SJ, Lee GT, Lee J-H, et al. Bone morphogenetic protein-6 induces the expression of inducible nitric oxide synthase in macrophages. Immunology. 2009; 128: e758-65.
86. Rocher C, Singla DK. SMAD-PI3K-Akt-mTOR pathway mediates BMP-7 polarization of monocytes into M2 macrophages. PLoS One. 2013; 8: e84009.
87. Yasmin N, Bauer T, Modak M, et al. Identification of bone morphogenetic protein 7 (BMP7) as an instructive factor for human epidermal Langerhans cell differentiation. J Exp Med. 2013/11/04. 2013; 210: 2597–2610.